Materials Characterization 157 (2019) 109879

Contents lists available at ScienceDirect

Materials Characterization

journal homepage: www.elsevier.com/locate/matchar

Interfacial reaction behavior and mechanical properties of pure aluminum and magnesium alloy dissimilar materials fabricated by hot press and heat treatment

Junko Umeda[a,*], Katsuyoshi Kondoh[a], Hiroyuki Sannomiya[a], Tachai Luangvaranunt[b], Makoto Takahashi[a], Hiroshi Nishikawa[a]

[a] Joining and Welding Research Institute, Osaka University, Japan
[b] Faculty of Engeering, Chulalongkorn University, Thailand

1. Introduction

A layered dissimilar material is a composite that consists of more than two different materials and exhibits a unique performance by the combination of different material properties. In particular, to achieve the balance between a weight reduction and high strength, the development of the advanced dissimilar materials is important in the industrial applications. A previous study on the impact energy absorption behavior of aluminum (Al) alloy and silicon carbide dissimilar materials with three-layer structures indicated that these dissimilar material plates have a higher energy absorption ability compared with the monolithic Al alloy [1]. The Charpy impact properties of ultrahigh carbon steel and Cu−Zn (brass) alloy layered dissimilar materials have also been investigated at ambient temperatures [2]. The results clarified that the impact toughness of the dissimilar materials was approximately 9 times higher than those of the monolithic ultrahigh carbon steel and brass alloy. The interfacial energy absorption mechanism due to delamination and separation behaviors was previously discussed in detail [3]. The properties of dissimilar materials strongly depend on their interface, and control of the interfacial microstructure is critical to producing layered materials with the excellent mechanical properties. The preparation conditions of dissimilar materials, particularly bonding temperature and time, are also important because the intermetallic compounds (IMCs) that form at interfaces during bonding are a dominant metallurgical factor in performance. For example, for a three-layer dissimilar material consisting of 5052 Al alloy/AZ31B Mg alloy/5052 Al alloy fabricated by a hot rolling process, there was a strong dependence of normal and shear bonding strengths on IMC layer thickness [4]. A suitable IMC thickness must be determined to obtain superior mechanical properties in dissimilar materials. Alternatively, from the viewpoint of solid-state dissimilar metal material preparation, the friction stir welding (FSW) technique has often been employed in previous studies [5,6]. Al alloy, AA2024 and Mg alloy, and ZE41 dissimilar jointed materials have been fabricated by FSW, and detailed discussions have been reported regarding the formation mechanisms of various IMCs in the joint stir zone and heat-affected zone. The solid-state reaction between the starting materials occurs easily at the interface due to the high pressure and high temperature fields during FSW. The plastic deformation caused by FSW, however, also leads to the mechanical breakage of in-situ formed IMC layers, which results in a uniform dispersion of fine IMC particles in the stir zone and heat-affected zone. In short, the strengthening mechanism of dissimilar jointed materials by both IMC dispersion and grain refinement have been the dominant focus in these previous studies. However, there has been no discussion regarding the effect of IMC layers on the mechanical strength of layered dissimilar materials.

Toward component weight reduction, this study employed a combination of pure Al and Mg alloys, where the commercial AZ31B (Mg-3%-1%Zn/wt%) was selected, as starting materials to fabricate dissimilar materials by hot pressing (HP) [7] and heat treatment (HT). The effects of HT temperature and time on the interfacial microstructures of AZ31B/pure Al/AZ31B dissimilar materials were discussed. In particular, the IMCs were identified by X-ray diffraction (XRD), and the formation mechanism and growth kinetics of IMCs layers were also discussed by using the activation energy of each compound. The microstructural analysis helped to clarify the effect of IMC layer thickness on the dynamic Charpy impact and static tensile properties of the dissimilar materials. In-situ scanning electron microscopy (SEM) observations of the fracture behavior during tensile tests was a powerful tool for understanding crack initiation and propagation phenomena near the interfaces between the IMC layers and each monolithic material.

2. Experimental procedure

2.1. Specimens fabrication

Pure Al (A1050, Fe: 0.26, Si: 0.1, Cu: 0.01, Al: Bal./mass%) plates

* Corresponding author.
E-mail address: umedaj@jwri.osaka-u.ac.jp (J. Umeda).

https://doi.org/10.1016/j.matchar.2019.109879
Received 15 April 2019; Received in revised form 15 August 2019; Accepted 19 August 2019
Available online 21 August 2019
1044-5803/

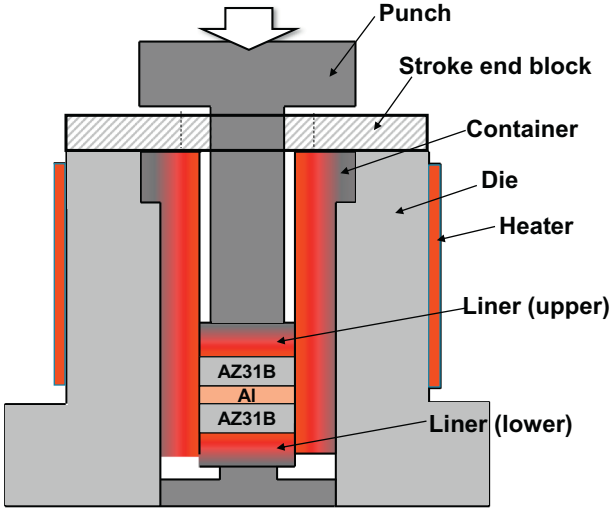

Fig. 1. Schematic illustration of direct bonding of Mg alloy (AZ31B) plates to pure Al plate by hot pressing process.

with thicknesses of 0.5 mm and commercial Mg alloy (AZ31B, Al: 2.95, Zn: 1.02, Mn: 0.3, Si: 0.015, Fe: 0.001, Cu < 0.01, Mg: Bal.) plates with thicknesses of 1.0 mm were used as the starting materials. Surface treatments by mirror polishing to prepare a smooth surface with no oxide film and by ultrasonic cleaning to completely remove oil and fats were conducted for each starting material. The three-ply plate specimens (AZ31B/Al/AZ31B) were pre-heated at 673 K for 180 s in an argon gas atmosphere as illustrated in Fig. 1. Then, they were immediately inserted into a container mold and consolidated by conventional HP, where the temperature of the mold and liners was 673 K and 600 MPa of pressure was applied to the specimens for 10 s by the upper punch. A previous study suggested that no new formation of IMCs at the interface of Al/Mg hot-rolled materials occurs after HT at 473 K [8]. Therefore, pre-heating and an HT temperature of 673 K were used in this study. Controlling the extent of plastic deformation induced by HP in the specimens was important for obtaining completely bonded materials at the interface. In this study, this was accurately controlled by using a stroke end block as shown in Fig. 1. HTs with various conditions (temperature: 473 K ~ 673 K, holding time at each temperature: 3.6 ks ~ 28.8 ks) under vacuum (~200 Pa) were applied to the bonded specimens to control the phases and thicknesses of the synthesized IMC layers.

2.2. Characteristics evaluation

For microstructural analysis, compositional images in backscattered electron mode were captured by field emission SEM, and energy dispersive X-ray spectroscopic (EDS) analysis was also carried out to investigate interfacial element mapping. Transmission electron microscopy (TEM) and XRD analyses were conducted for phase identification of the IMC layers. To evaluate the mechanical properties of the bonded dissimilar materials, Charpy U-notch impact tests (maximum impact energy: 27.4 mJ) and tensile tests (strain rate: $5 \times 10^{-4}\,s^{-1}$) were carried out at room temperature. Fig. 2 illustrates the specimen geometry used in the Charpy impact tests and the test procedure. In this study, the total energy schematically shown in Fig. 2 was used to evaluate the impact toughness of the specimens. After both tests, the interfacial fracture profiles of the specimens were also investigated by SEM.

3. Results and discussion

3.1. Microstructural analysis of IMC layers at interfaces of dissimilar materials

Fig. 3 shows the SEM images of the microstructures at the interface between the pure Al and AZ31B plates of the as-HPed specimen and those after HT with various conditions. It is obvious that the as-HPed (a) and HTed at 598 K for 3.6 ks (b) materials showed no formation of interfacial IMCs. As shown in (c-1), elliptical or spherical IMCs discontinuously formed at the interface after HT at 598 K for 7.2 ks. This suggests the possibility of synthesizing IMCs via solid-state reaction during a long HT period at 598 K. According to the Al—Mg binary phase diagram [9], the solubility of Mg in Al and that of Al in Mg are approximately 9.0 at.% and 6.0 at.%, respectively, at 598 K. With an increase in HT time, the interdiffusion between pure Al and AZ31B proceeded gradually through the interface, and each solid solution concentration over the above mentioned solubility resulted in the formation of IMC particles, as schematically illustrated in Fig. 3 (c-2). Finally, layered IMCs with a uniform thickness formed at the interface upon HT at 598 K for 14.4 ks, as shown in Fig. 3 (d-1) and (d-2), because the diffusion of Al and Mg atoms occurred along the interface [4]. When the HT temperature was increased from 623 K to 673 K, the thickness of the IMC layers increased and two different layers clearly formed. In the cases of HT at 648 K for 14.4 ks and at 673 K for 7.2 ks/14.4 ks, however, large cracks propagated inside the layers along the interfaces because of thermal stress induced by thermal expansion differences between the two brittle IMC layers during long HT times and subsequent cooling to room temperature.

XRD and electron-probe X-ray microanalysis (EPMA) were carried out to identify the form of each interfacial IMC layer in the Al/AZ31B dissimilar materials after HT at 673 K for 3.6 ks. As shown in Fig. 4 (a), in addition to Al and Mg diffraction peaks for the starting materials, peaks corresponding to Al_3Mg_2 (β-phase) and $Al_{12}Mg_{17}$ (γ-phase) were clearly detected at the interface. Fig. 4 (b) shows the EPMA line analysis results of Al and Mg elements across the interface. The IMC layer next to the AZ31B plate with an approximate thickness of 15 μm ("layer-1")

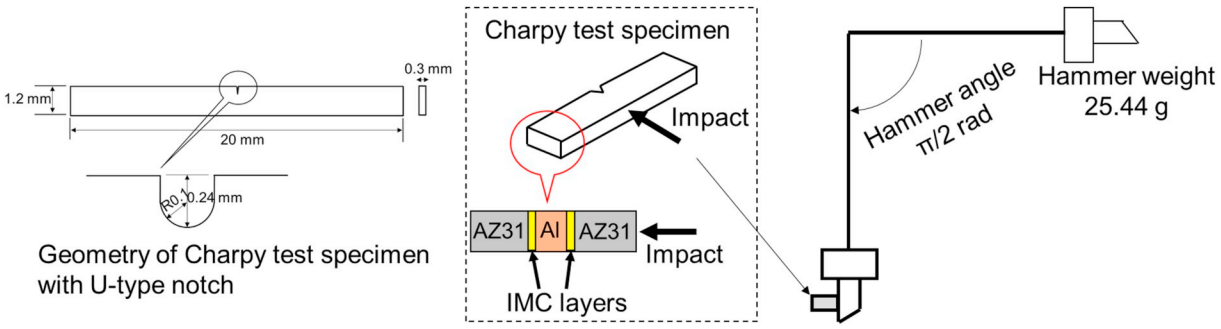

Fig. 2. Schematic illustration of micro Charpy impact test and its specimen geometry of AZ31B/Al/AZ31B layer-structure dissimilar material.

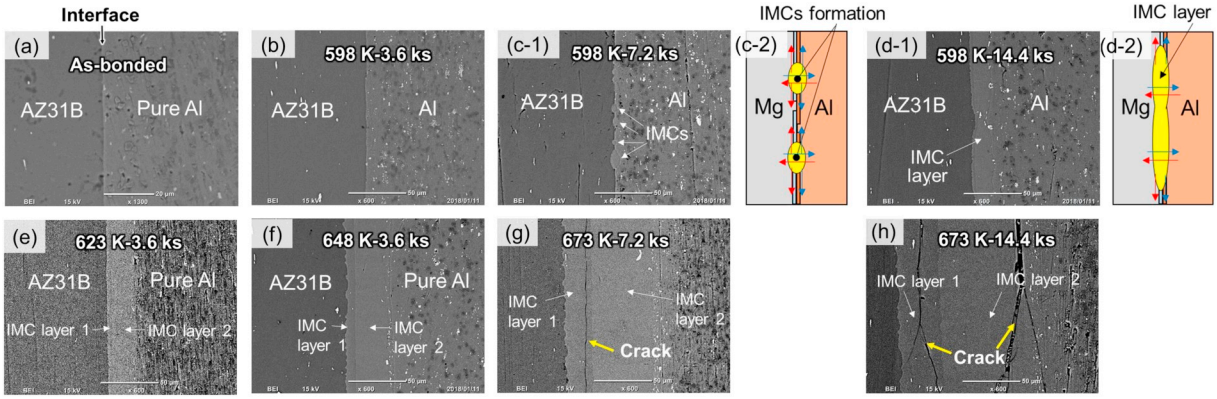

Fig. 3. SEM observation on AZ31B/Al bonding interfaces of as-bonded dissimilar material (a) and those via various heat treatment conditions (b)~(h). Illustrations of intermetallic compounds formation at interface is also attached as (c-2) and (d-2).

was rich in Mg, whereas that close to pure Al with a thickness of 50 μm ("layer-2") was poor in Mg. The point analysis results for No. 1–7 in Fig. 4 (b-1) are summarized in the table in Fig. 4. At points 2 and 3 located in layer-1, the Al and Mg contents were 40–44 at.% and 56–60 at.%, respectively. These atomic ratios are close to the chemical composition of $Al_{12}Mg_{17}$ (Al: Mg = 41.4: 58.6 at.%). Similarly, the ratio of Al to Mg at points 4 and 5 located in layer-2 was 60 at.% to 40 at.%, which is in very good agreement with that of Al_3Mg_2 (Al: Mg = 60: 40 at.%). For further microstructural investigation, TEM-EDS analysis was conducted, which successfully identified layer-1 and layer-2 as $Al_{12}Mg_{17}$ (γ-phase) and Al_3Mg_2 (β-phase), respectively, by calculation of the interplanar *d*-spacings using the diffraction patterns from points 1 and 2 shown in Fig. 5 (a).

3.2. Growth mechanism of interfacial IMC layers by HT

According to the microstructural observation (Fig. 3) and phase identification (Figs. 4 and 5) results, Fig. 6 shows the relationship between IMC layer thickness (X) and the square root of the holding time ($\sqrt{t}$) of the (a) Al_3Mg_2 (β-phase) and (b) $Al_{12}Mg_{17}$ (γ-phase) layers resulting from different HT conditions. Both IMC layers clearly increased in thickness with increasing holding time and HT temperature. In addition, the increase in thickness of the Al_3Mg_2 layer was larger than that of the $Al_{12}Mg_{17}$ layer. According to the relationships of both IMC layers shown in Fig. 6, the below equation was obtained [10]:

$$X = \sqrt{Dt}, \tag{1}$$

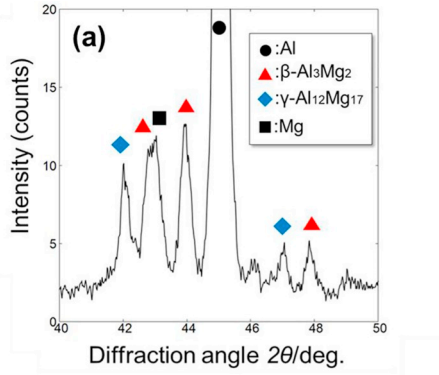

No.	Mg (at .%)	Al (at .%)	Position
1	95.47	4.53	AZ31B
2	60.38	39.62	IMC layer (AZ31B side)
3	56.30	43.70	IMC layer (AZ31B side)
4	40.22	59.78	IMC layer (Al side)
5	39.81	60.19	IMC layer (Al side)
6	5.05	94.95	Al
7	0.02	99.98	Al

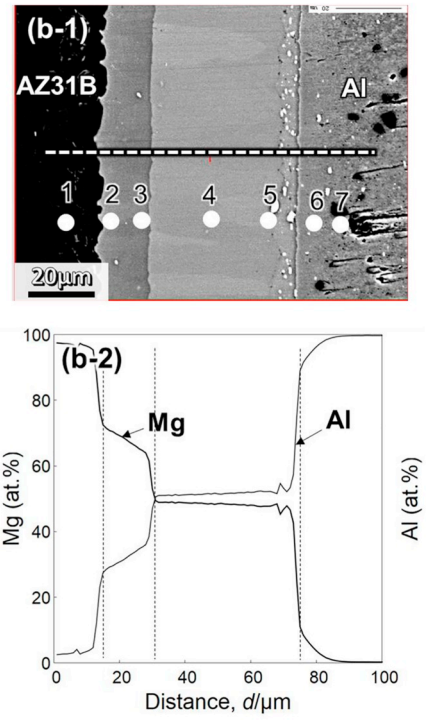

Fig. 4. XRD profile (a), EPMA line scanning analysis result (b) and element point analysis of AZ31B/Al interface of dissimilar material after heat treatment in vacuum at 673 K for 3.6 ks.

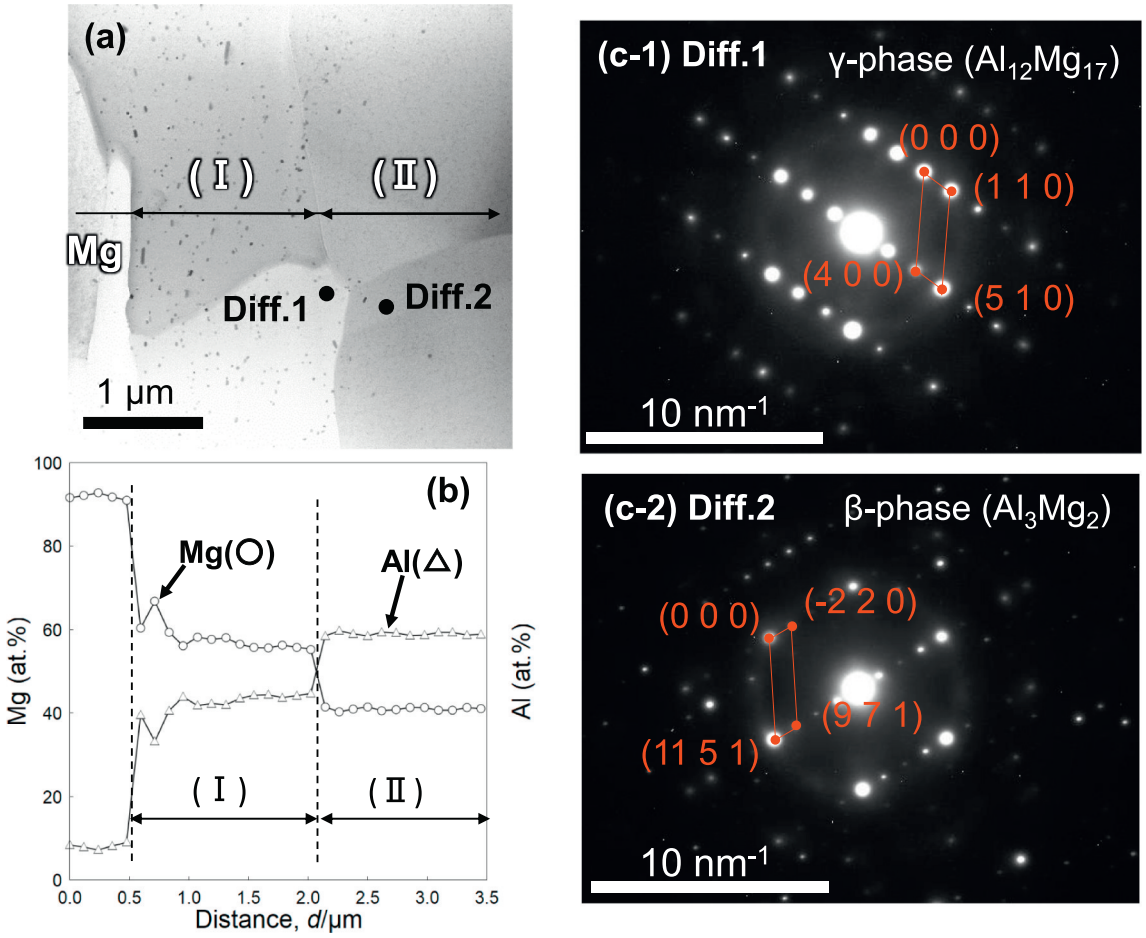

Fig. 5. TEM-EDS line scanning analysis and TEM diffraction analysis results of interface of dissimilar material after annealing treatment at 598 K for 14.4 ks. Table shows calculation results of interplanars (d-spacing) using diffraction patters at point 1 and 2 shown in Fig. 5 (a).

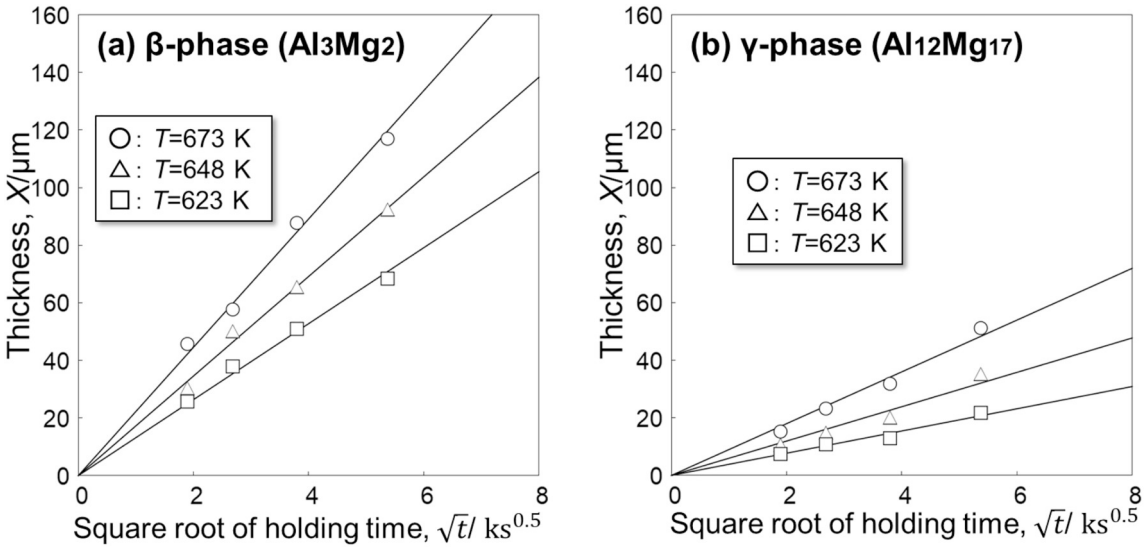

Fig. 6. Relationship between each IMC layer thickness and square root of holding time at various HT temperatures of dissimilar materials: β-phase of Al_3Mg_2 (a) and γ-phase of $Al_{12}Mg_{17}$ (b).

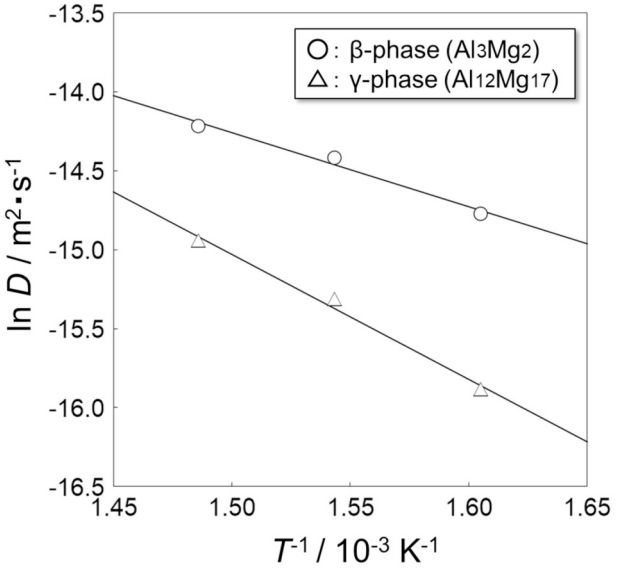

Fig. 7. Arrhenius plots for growth rate of β-phase (Al_3Mg_2) and γ-phase ($Al_{12}Mg_{17}$) layers at interface of AZ31B/Al/AZ31B dissimilar materials after HT.

where X (m) is the layer thickness at time t and D (m^2/s) is the reaction rate constant.

To calculate the activation energy necessary for the growth of each IMC layer during HT [11], the Arrhenius plots [12] shown in Fig. 7 were composed using the gradient of the straight data line under each temperature obtained in Fig. 6. The activation energy can be calculated by expressing the Arrhenius equation, Eq. (2), as a natural logarithm, Eq. (3), with which the growth rate of each IMC layer at certain temperatures can be estimated [12].

$$D = D_0 \exp\left(-\frac{Q}{RT}\right), \tag{2}$$

$$\ln D = \ln D_0 - \frac{Q}{RT}, \tag{3}$$

where D is the diffusion coefficient (m^2/s), D_0 is the diffusion constant (m^2/s), Q is the activation energy (J/mol), R is the gas constant (=8.314 J/mol·K), and T is temperature (K).

In Fig. 7, the y-axis, $ln\ D$, is derived from the slope of each straight line obtained by the least squares method from the relationship between the thickness of each IMC layer (Fig. 6) and square root of the retention time $\sqrt{t}$, and the x-axis is the reciprocal $T^{-}1$ of each HT temperature. The apparent activation energies for the growth of β-phase and γ-phase layers calculated from the Arrhenius plot were 39.0 kJ/mol and 65.8 kJ/mol, respectively. This implies that the β-

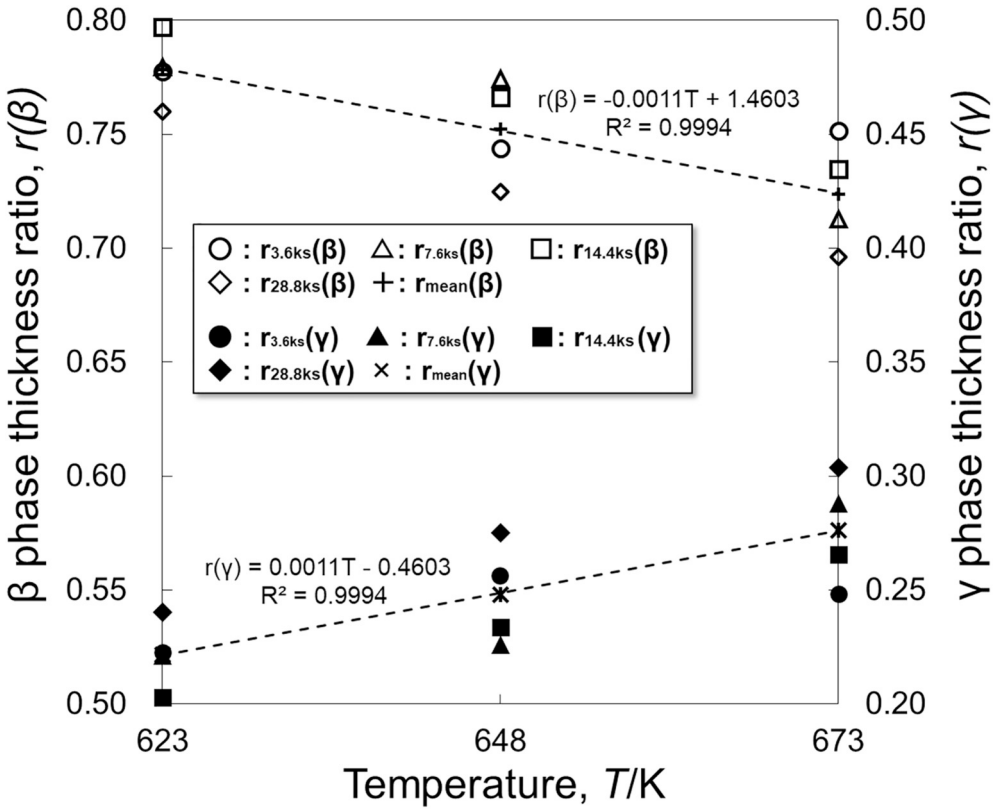

Fig. 8. Dependence of each intermetallic compound layer thickness ratio on HT temperature.

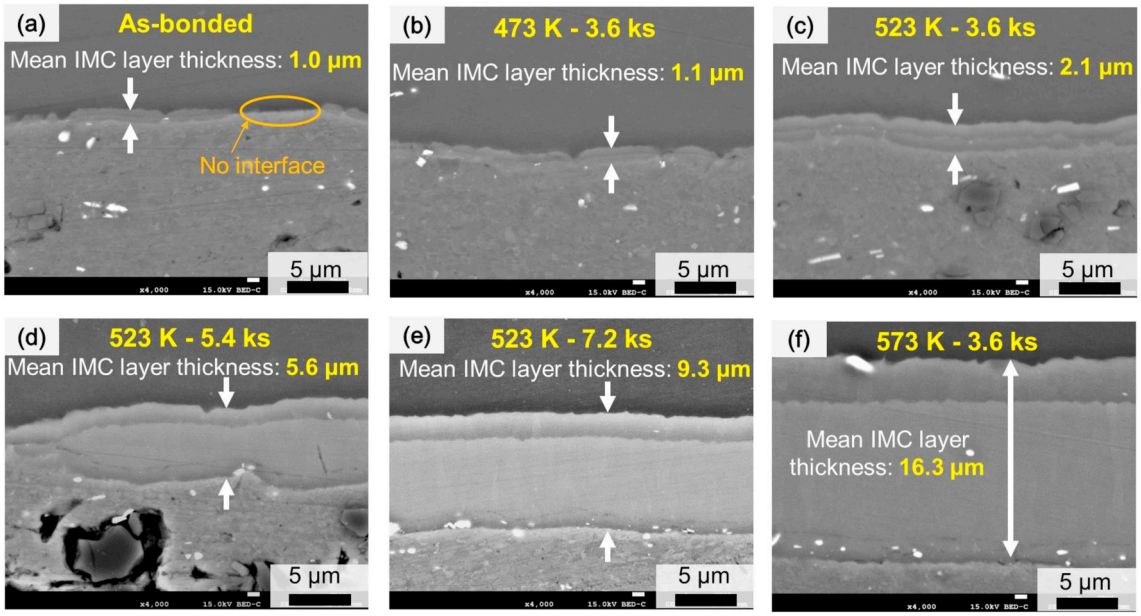

Fig. 9. SEM micrographs of AZ31B/Al interface via various HT conditions: as-bonded dissimilar material (a), heat treated at 473 K for 3.6 ks (b), 523 K for 3.6 ks (c), 523 K for 5.4 ks (d), 523 K for 7.2 ks (e) and 573 K for 3.6 ks (f).

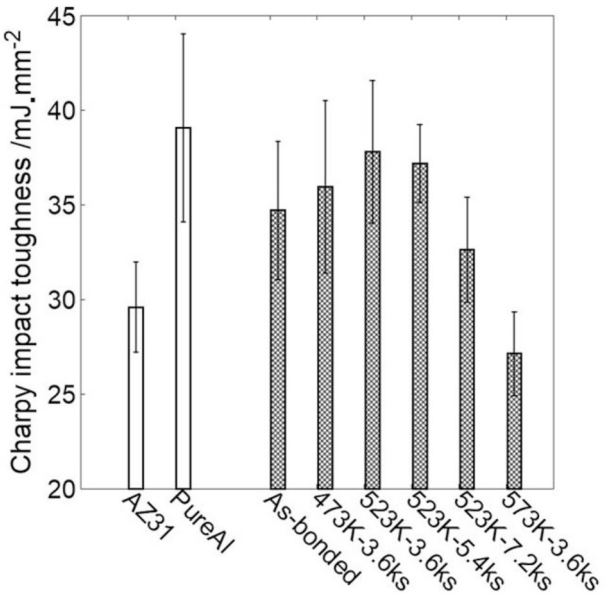

Fig. 10. Micro Charpy impact test results of monolithic AZ31B, pure Al and AZ31B/Al/AZ31B layer-structure dissimilar materials after HT.

phase grows more easily at the interface of the dissimilar material compared with the γ-phase. The thicknesses of the β- and γ-phases synthesized at each HT temperature were denoted as $d(\beta)$ and $d(\gamma)$, and the ratio of each layer thickness to the total thickness of the IMC layers was determined as follows:

$$r(\beta) = d(\beta)/(d(\beta) + d(\gamma)),\ r(\gamma) = d(\gamma)/(d(\beta) + d(\gamma)). \quad (4)$$

Fig. 8 shows the relationship between each layer thickness ratio and HT temperature, where the subscript of each symbol indicates the holding time at the HT temperature and the subscript "mean" indicates an average layer thickness ratio. With an increase in temperature, $r\text{mean}(\beta)$ gradually decreased, whereas $r\text{mean}(\gamma)$ increased. According to the relationship between ln D and $T^{-}1$ shown in Fig. 7, the difference between $ln\ D$ (= −14.22) in the β-phase and $ln\ D$ (= −14.95) in the γ-phase at T = 673 K was 0.73 m^2/s. On the other hand, the difference between $ln\ D$ (= −14.77) in the β-phase and $ln\ D$ (= −15.88) in the γ-phase at T = 623 K was 1.12 m^2/s. As shown in Fig. 6, the present data have a linear relationship in the Arrhenius plot. Therefore, the formation and growth of each IMC phase is based on a thermally activated diffusion mechanism, and with an increase in HT temperature, the diffusion coefficient of each phase increases rapidly. Because the rate of increase with temperature is different, however, the relative difference between the phases decreases. Accordingly, as the HT temperature increases, $r\text{mean}(\beta)$ decreases and $r\text{mean}(\gamma)$ tends to increase in the formation of interfacial IMC layers.

In the range of HT experimental conditions used in this study, the ratio of β-phase thickness to the total thickness of both IMC layers was much larger than that of the γ-phase layer. As a further consideration, the temperature at which the thickness ratios, $r(\beta)$ and $r(\gamma)$, intersect was determined as T = 873 K, as shown in Fig. 8. The Al—Mg binary phase diagram suggests that the melting point, T_m, of the β-phase (Al_3Mg_2) is 723 K and that of the γ-phase ($Al_{12}Mg_{17}$) is approximately 733 K. That is, it is not possible for $r(\beta)$ and $r(\gamma)$ to be the same in solid-state conditions. In addition, the $r(\gamma)$ limit of the β-phase (Al_3Mg_2) at T_m (= 723 K) is $r(\gamma)$ = 0.335. In the solid-state synthesis range of these compounds, it is found that the proportion of β-phase to the total IMC

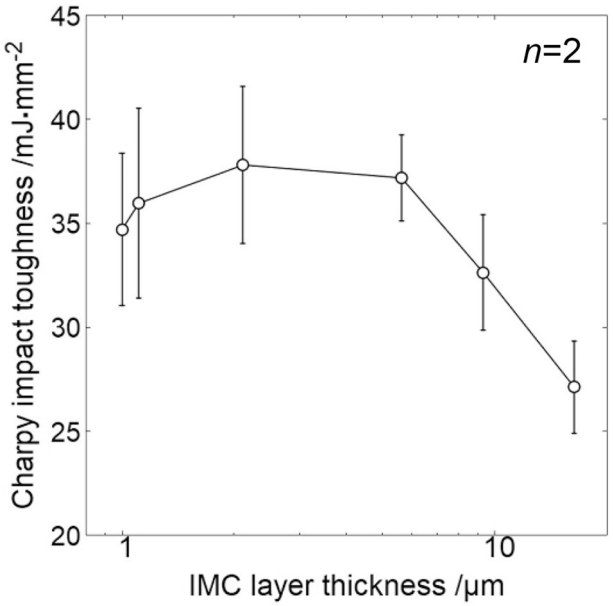

Fig. 11. Dependence of Charpy impact toughness on total thickness of IMC layers formed at interface.

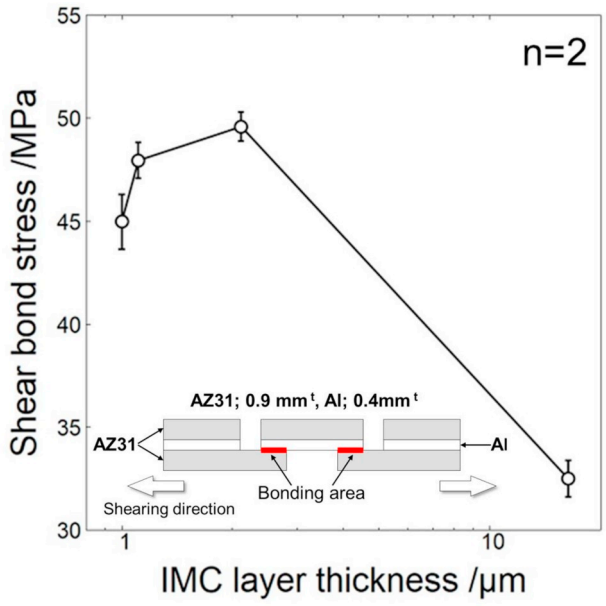

Fig. 12. Dependence of shear bond strength of AZ31B/Al bonded materials on IMC layer thickness. Details of test specimen and evaluation are also inserted in test results.

layer thickness is always larger than that of the γ-phase.

3.3. Mechanical property evaluation of AZ31B/Al/AZ31B layered dissimilar materials

Charpy impact tests and static tensile tests were conducted to investigate the effect of IMC layer thickness on the mechanical properties of AZ31B/Al/AZ31B layered dissimilar materials induced by different HT conditions after the HP process. After fabrication of the dissimilar materials by HP, the HT conditions of 473 K, 523 K, and 573 K for 3.6 ks under vacuum and 523 K for 5.4 ks and 7.2 ks under vacuum were employed. Fig. 9 shows the SEM images of the AZ31B/Al interface after various HT conditions and the mean IMC layer thickness of each bonded material, which is the total thickness of the β- (Al_3Mg_2) and γ-phase ($Al_{12}Mg_{17}$) layers. In the as-HPed material with no HT (a), an IMC layer with a thickness of approximately 1 μm formed discontinuously at the interface. The other dissimilar materials contained continuously synthesized layers with uniform thicknesses. Fig. 10 shows the Charpy impact test results of the specimens, where A31B and pure Al plates were also evaluated as reference materials. First, the pure Al single specimen had the highest impact toughness, which was approximately 32% higher than that of the AZ31B single plate, although its variation was large. All the dissimilar materials, except for the specimen subjected to HT at 573 K for 3.6 ks, had much higher impact toughnesses than the AZ31B single specimen. Fig. 11 shows the relationship between the Charpy impact toughnesses of the AZ31B/Al/AZ31B layered bonded materials and total IMC layer thickness determined according to these results. When the IMC layer thickness was between approximately 1 μm and 2 μm, the Charpy impact toughness of the dissimilar material increased as layer thickness increased. However, the impact toughness decreased for bonded materials with relatively thick layers from approximately 9 μm to 16 μm. Similarly, a previous

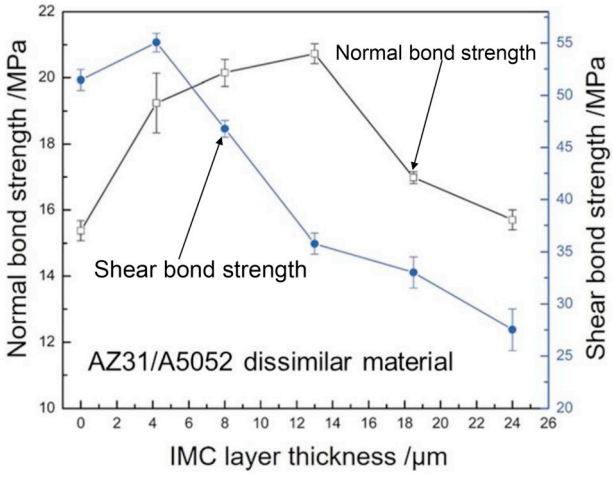

Fig. 13. Dependence of normal and shear bond strength on IMC layer thickness of AZ31/A5052 dissimilar materials fabricated by hot rolling process [4].

study [3] reported that the thickness of the IMC layer formed at the bonding interface greatly affects the interfacial bonding strength between different phases of dissimilar materials due to the brittleness of the IMCs.

Next, shear test specimens were machined from the as-HPed AZ31B/Al/AZ31B dissimilar material and those subjected to HT at 473 K, 523 K, and 573 K to quantitatively evaluate the bonding strength of the AZ31B/Al joint parts. As shown in Fig. 12, the shear bond stress of the AZ31B/Al joint increased for IMC layer thicknesses less than approximately 2 μm. The stress, however, was the smallest for a

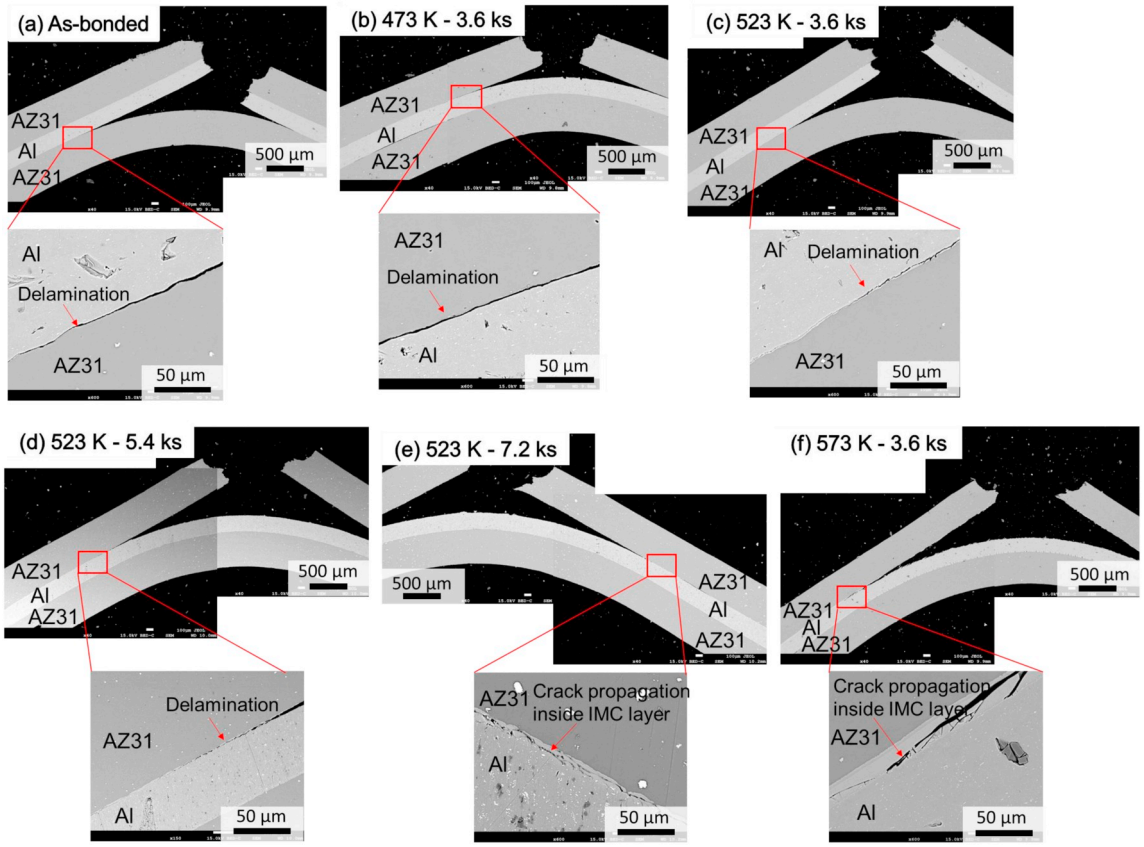

Fig. 14. Fractured profiles of AZ31B/Al/AZ31B layer-structure dissimilar materials after micro Charpy impact test: as-bonded dissimilar material (a), heat treated at 473 K for 3.6 ks (b), 523 K for 3.6 ks (c), 523 K for 5.4 ks (d), 523 K for 7.2 ks (e) and 573 K for 3.6 ks (f)

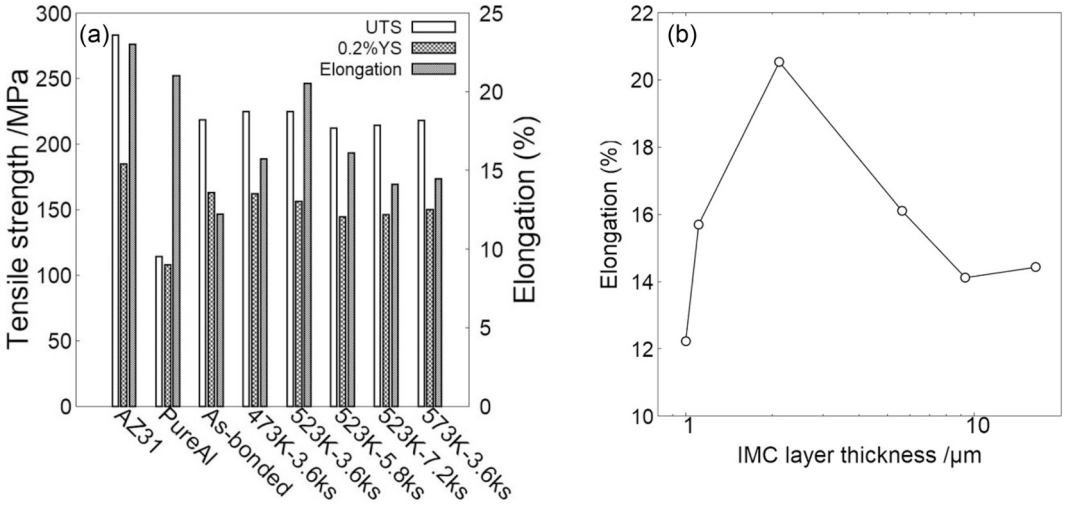

Fig. 15. Tensile properties of AZ31B/Al/AZ31B dissimilar materials after HT with various conditions compared to AZ31B and pure Al plates (a) and elongation dependence on IMC layer thickness of dissimilar materials (b).

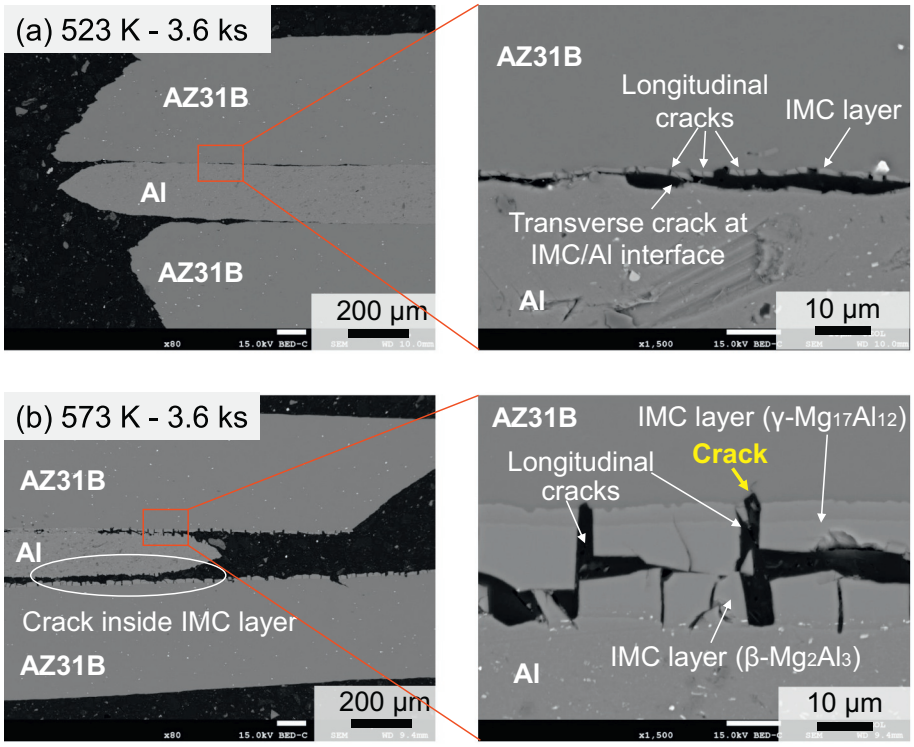

Fig. 16. Fractured profiles of AZ31B/Al/AZ31B dissimilar materials after tensile test: 523 K for 3.6 ks (a) and 573 K for 3.6 ks (b).

relatively large layer thickness of approximately 16 μm, which agreed with the relationship between Charpy impact toughness and IMC layer thickness shown in Fig. 11. Furthermore, a previous study [4] reported the relationship between shear bond strength (closed circles, ●) and IMC layer thickness at the bonding interface of AZ31/A5052 dissimilar clad materials, as shown in Fig. 13. The results indicated that shear bonding strength gradually increased when the thickness was 4 μm or less and decreased drastically when the thickness was over 4 μm. This is in good agreement with the shear test results from this study shown in Fig. 12.

The crack propagation behavior was investigated by SEM observations of laminated sections of the specimens after Charpy impact testing to clarify why the AZ31B/Al/AZ31B dissimilar material subjected to HT at 573 K with an IMC layer thickness of 16.3 μm had the lowest impact fracture property. As shown in Fig. 14 (a) ~ (d), the bonded specimens with IMC layer thicknesses of 1 μm ~ 6 μm clearly showed interfacial delamination behavior. For the dissimilar materials with relatively large layer thicknesses of 9 μm and 16 μm shown in (e) and (f), however, crack propagation occurred inside the brittle IMC layers, but no interfacial delamination was observed because the thick IMC layers easily became a path for crack propagation. In addition, since the IMC layer has a high elastic modulus compared with those of monolithic AZ31B and pure Al plates, a larger tensile stress is applied to the inside of the layer with an increase in layer thickness when bending deformation is applied. As a result, the dissimilar material with a 16.3 μm IMC layer had the lowest impact toughness of all the specimens. In a previous study [3], the toughening mechanism of laminate materials was investigated by applying impact energy and introducing 4 types of fracturing behavior: crack deflection, crack blunting, crack bridging, and stress redistribution. According to the above discussions of crack propagation behavior at the interface of AZ31B/Al/AZ31B dissimilar materials with relatively thick IMC layers, the crack initiated from the brittle IMC layer and propagated inside the layer, not at the interface. This is mainly because of the residual stress caused by a thermal expansion difference between the IMC layers and the metal (AZ31B and Al) plates. As a result, crack-deflection-like fracturing occurred at the interface of this bonded dissimilar material with IMC layers.

Fig. 15 (a) shows the tensile test results of the AZ31B/Al/AZ31B dissimilar materials compared with those of the monolithic AZ31B and pure Al plates, where the mean values of 2 test specimens were used. The results clarified that the ultimate tensile strength and yield stress (0.2%YS) were almost constant regardless of IMC layer thickness induced by different HT conditions. As shown in Fig. 15 (b), however, the elongation to failure did depend on layer thickness. In the thickness range of 1 μm ~ 2 μm, the elongation gradually increased with increasing thickness because the interfacial shear bonding strength also increased, as shown in Fig. 12. In order to analyze the factors reducing the elongation of the bonded specimens with IMC layer thicknesses over 5 μm, the fractured profiles, in particular the micro-crack initiation behaviors, at the interfaces of the tensile specimens HTed at 523 K for

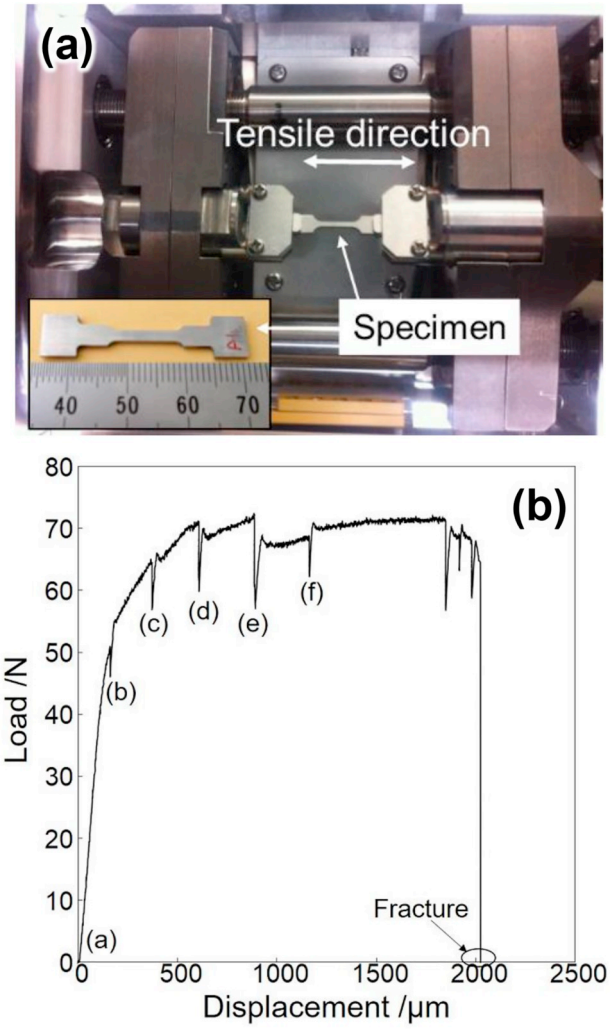

Fig. 17. Small tensile test system installed in SEM equipment (a) and example of load-displacement profile in tensile test of AZ31B/Al/AZ31B dissimilar bonded material with HT at 573 K for 3.6 ks (b).

3.6 ks (a) and 573 K for 3.6 ks (b) were investigated by SEM observation, as shown in Fig. 16. In the specimen with an IMC layer thickness of 2.1 μm (a), numerous micro-cracks perpendicular to the IMC layer ("longitudinal cracks") were detected inside the layer, and the main fracture was due to a transverse (parallel) crack at the interface between the IMC layer and pure Al plate. On the other hand, the specimen with an IMC layer thickness of 16.3 μm (b) showed not only longitudinal cracks but also large transverse cracks inside the β-phase (Al_3Mg_2) layer. Longitudinal crack propagation, however, was completely halted at both the monolithic AZ31B and pure Al plates. According to these results, the poor elongation of the bonded specimens with relatively thick IMC layers was mainly due to large transverse cracks inside the brittle IMC layer.

To further investigate the crack initiation and propagation behavior of the bonded specimen with a relatively thick IMC layer of 16.3 μm shown in Fig. 16 (b), in-situ SEM observations of the fracturing phenomenon during tensile testing were carried out. As shown in Fig. 17 (a), a small tensile test system was installed in the SEM equipment to evaluate the fracturing behavior in this study. An example of the load-displacement profile from this tensile test of the AZ31B/Al/AZ31B dissimilar bonded material subjected to HT at 573 K for 3.6 ks is shown in Fig. 17 (b). During the tensile test, the cross-head was temporarily stopped to observe interfacial fractures at each point (a)~(f). Fig. 18 (a) shows the well-bonded AZ31B/Al interface, where no cracks were present and an IMC layer with a thickness of approximately 15 μm existed between both monolithic plates, which was close to the layer thickness shown in Fig. 9 (f). When an approximately 50 N load was applied at point (b) in Fig. 17 (b), some longitudinal cracks initiated inside the IMC layer, as shown in Fig. 18 (b). With an increase in the applied load from 65 N to 70 N (corresponding to points (c) and (d), respectively), the transverse crack mainly propagated inside the IMC layer, and the crack opening displacement became increasingly larger, as shown in Fig. 18 (c) and (d). The results also clarified that the small longitudinal cracks and main transverse crack never propagated into the ductile monolithic materials of the AZ31B and pure Al plates with increasing displacement, as shown in Fig. 18 (e) and (f). This fracturing behavior is in good agreement with the SEM observations shown in Fig. 16 (b). The results indicated that the plastic deformation ability, particularly the elongation, of the dissimilar material with a relatively thick IMC layer was strongly limited by the brittleness of the β- and γ-phases.

4. Conclusions

The formation mechanism and growth kinetics of IMCs at the interface of AZ31B/pure Al/AZ31B layered dissimilar materials after HT with various conditions were quantitatively discussed by using the activation energy for IMC layer growth calculated from the Arrhenius plot and XRD, SEM, and TEM analyses. The apparent activation energies for the growth of β-phase (Al_3Mg_2) and γ-phase ($Al_{12}Mg_{17}$) layers were 39.0 kJ/mol and 65.8 kJ/mol, respectively; that is, the β-phase grew more easily at the interface of the dissimilar material compared with the γ-phase. Regarding the dynamic impact properties of the dissimilar materials and their fracturing behavior, a maximum Charpy impact toughness was obtained for an IMC layer thickness of approximately 2 μm, and the toughness drastically decreased with increasing IMC layer thickness. In-situ SEM observations during tensile testing indicated that cracks propagated inside the brittle IMC layers, but no interfacial delamination was observed for dissimilar materials with relatively thick IMC layers. It was concluded that these Mg—Al dissimilar materials showed the important advantages to reduce the component weight and improve both strength, ductility and toughness compared to the conventional Mg or Al alloys.

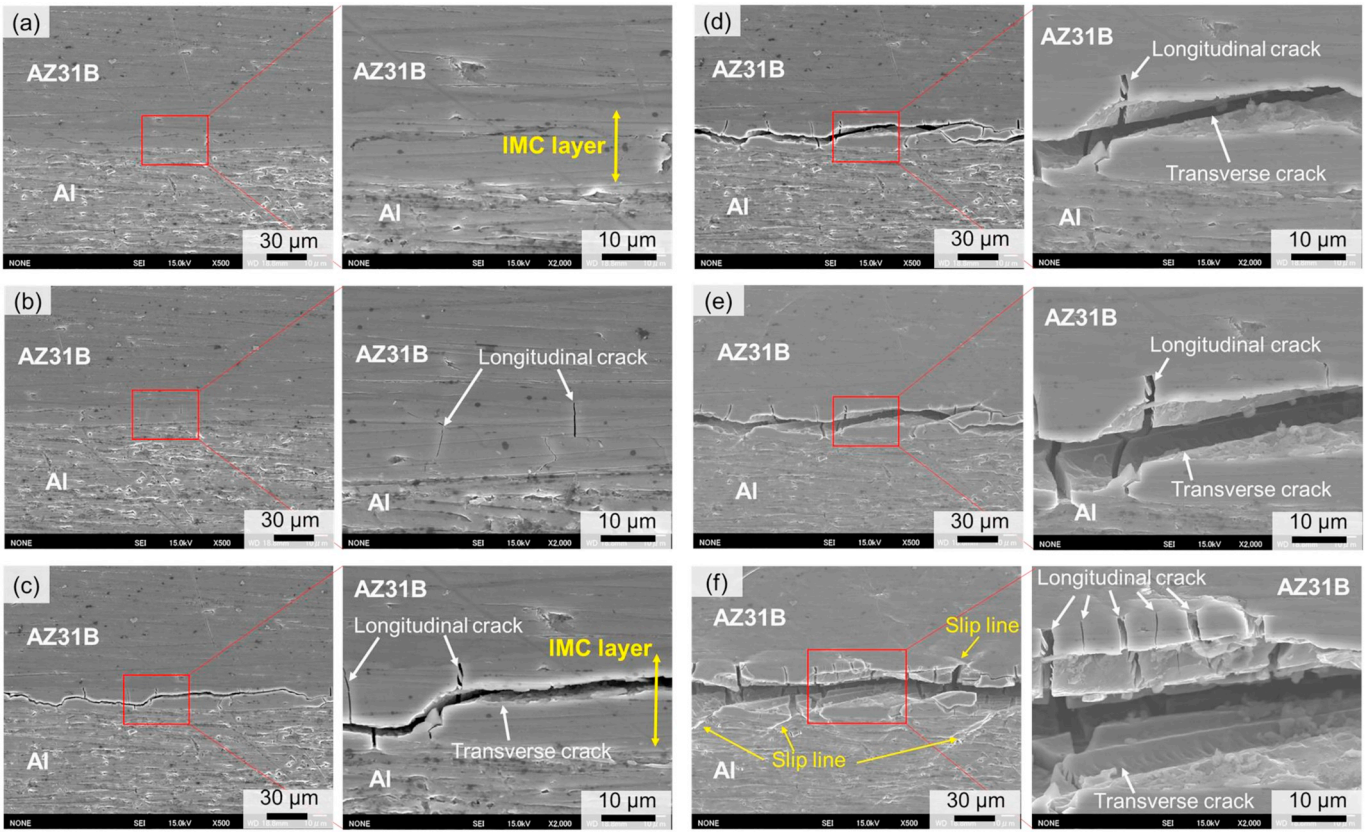

Fig. 18. Crack initiation and propagation inside IMC layers formed at interface during in-situ tensile test at (a) ~ (f) points in Fig. 17 (b).

Acknowledgements

This study was financially supported by the Project to Create Research and Educational Hubs for Innovative Manufacturing in Asia and the research program on establishment of a virtual joint laboratory between RMIT and JWRI, Osaka University. The authors showed great thanks for Mr. Hiroyuki Sannomiya for his supports in this experiment.

Declaration of competing interest

None.

References

[1] D.R. Lesuer, C.K. Syn, O.D. Sherby, J. Wadsworth, Laminated metals composites—Fracture and ballistic impact behavior, Third Pacific Rim Conference on Advanced Materials and Processing, Honolulu, Hawaii, USA, July 12–16, 1998 (UCRL-JC-129676).

[2] S. Lee, T. Oyama, J. Wadsworth, O.D. Sherby, Impact properties of a laminated composite based on ultrahigh carbon steel and brass, Mater. Sci. Eng. A 154 (1992) 133–137, https://doi.org/10.1016/0921-5093(92)90338-2.

[3] D.R. Lesuer, C.K. Syn, O.D. Sherby, J. Wadsworth, J.J. Lewandowski, W.H. Hunt, Mechanical behavior of laminated metal composites, Int. Mater. Rev. 41 (1996) 169–197, https://doi.org/10.1179/imr.1996.41.5.169.

[4] J.J. Zhang, W. Liang, H.T. Li, Effect of thickness of interfacial intermetallic compound layers on the interfacial bond strength and the uniaxial tensile behaviour of 5052 Al/AZ31B Mg/5052 Al clad sheets, RSC Adv. 5 (2015) 104954–104959, https://doi.org/10.1039/C5RA15357C.

[5] V. Paradiso, F. Rubino, P. Carlone, G.S. Palazzo, Magnesium and aluminium alloys dissimilar joining by friction stir welding, Procedia Eng 183 (2017) 239–244, https://doi.org/10.1016/j.proeng.2017.04.028.

[6] L. Liu, D. Ren, F. Liu, A review of dissimilar welding techniques for magnesium alloys to aluminum alloys, Materials 7 (2014) 3735–3757, https://doi.org/10.3390/ma7053735.

[7] T. Nakamura, K. Hayakawa, S. Tanaka, H. Imaizumi, Y. Nakagawa, Bonding characteristics of various metals by DC pulse resistance heat pressure welding, Mater. Trans. 46 (2005) 292–297, https://doi.org/10.2320/matertrans.46.292.

[8] C. Luo, W. Liang, Z. Chen, J. Zhang, C. Chi, F. Yang, Effect of high temperature annealing and subsequent hot rolling on microstructural evolution at the bond-interface of Al/Mg/Al alloy laminated composites, Mater. Charact. 84 (2013) 34–40, https://doi.org/10.1016/j.matchar.2013.07.007.

[9] J.L. Murray, The Al–mg (aluminum–magnesium) system, Bull. Alloy Phase Diagrams 3 (1982) 60–74, https://doi.org/10.1007/BF02873413.

[10] K.H. Prakash, T. Sritharan, Effects of solid-state annealing on the interfacial intermetallics between tin-lead solders and copper, J. Electron. Mater. 32 (2003) 939–947, https://doi.org/10.1007/s11664-003-0227-7.

[11] R.J. Silbey, R.A. Alberty, M.G. Bawendi, Physical Chemistry, Wiley, New York, 1997.

[12] S. Arrhenius, Über die reaktionsgeschwindigkeit bei der inversion von rohrzucker durch säuren, Z. Phys. Chem. 4 (1889) 226–248, https://doi.org/10.1515/zpch-1889-0416.